Deformation and Orientation of Flexible Polymers in Solution under Shear Flow: A New Picture for Intermediate Reduced Shear Rates

Carlo Pierleoni*,† and Jean-Paul Ryckaert*,‡

Condensed Matter Statistical Physics, Université Libre de Bruxelles, CP 223, 1050 Brussels, Belgium

Received November 29, 1994; Revised Manuscript Received February 23, 1995[⊗]

ABSTRACT: An N-bead chain ($9 \leq N \leq 50$) in solvent subjected to steady shear flow with shear rate $\dot{\gamma}$ is treated by molecular dynamics simulation in order to analyze in a systematic way the deformation and the alignment of polymers in such a nonequilibrium stationary state. The reduced shear rate $\beta = \dot{\gamma}\tau_N$, where τ_N is the chain longest relaxation time, is the key quantity used to connect real experiments and simulations. Our results for good solvent conditions suggest that chains of various lengths do obey anisotropic scaling laws; β-dependent Flory exponents for each principal axis of the gyration tensor are extracted from the global dimensions of the deformed chains and from their internal spatial correlations. The good agreement between the molecular dynamics data with results of experiments on dilute solutions of polymers subject to Couette flow supports the proposed scaling picture.

1. Introduction

The deformation and the orientation of flexible polymers in various flow fields is a longstanding problem of polymer science. Even for dilute polymer solutions, which is a single-chain problem, only the gross features of the chain structure in various types of flow (elongational or shear, time independent or stationary, etc.) are settled and they confirm intuitive expectations. A deeper understanding is often prevented by the inherent difficulties encountered by the theory when dealing with nonequilibrium problems and, on the experimental side, by the difficulties in combining a flow cell with a suitable detector geometry.

In the particular case of a shear flow, one is interested in following both the overall deformation and orientation of the chain and its internal structure as a function of shear rate, $\dot{\gamma}$. The evolution of the chain structure with the flow intensity has been monitored by several experimental techniques. Early investigations were performed by measuring flow birefringence effects[1] while nowadays more powerful neutron and light scattering techniques are used. With neutrons, one can access the internal structure of the chain and, provided the chain is sufficiently short, its global dimensions.[2] On the other hand, typical light scattering wavelengths require long polymers and only their global structure can be probed.[3,4] Results for different chain lengths can be readily compared because the deformation and the orientational properties should depend essentially on the reduced shear rate, $\beta = \dot{\gamma}\tau$, where τ is the longest relaxation time of the chain at equilibrium. Experimentally accessible values of β are limited by the unfavorable signal to noise ratio at small β and by the onset of flow instabilities and chain fracture effects at high β. The range of shear rates experimentally investigated so far is $0.2 < \beta < 30$. The picture which emerges is as follows. The chain, which on average is spherically symmetrical at equilibrium, becomes ellipsoidal under shear. Its principal axes in the flow plane are oriented with respect to the flow direction by an angle (the orientation angle defined in eq 4 below) which decreases from $\pi/4$ to zero with increasing β. The size of the chain is greatly increased in the flow direction while in the other two directions a small contraction is observed at high β.[2-4]

Theoretical predictions for the chain behavior in shear flow has been given for various chain models. Normal mode analysis[5-7] and renormalization group theory techniques[8-13] have been used on harmonic chains with or without excluded volume (EV) and with or without preaveraged hydrodynamic interaction (HI) effects. These methods predict a linear dependence on β for the orientation and a quadratic dependence on β for the deformations in the flow plane, while in the out-of-plane direction the chain size remains at its equilibrium value. Such predictions are in qualitative agreement with experimental data for $\beta \leq 1$, but the large experimental noise in this range of β does not make it possible to discriminate between the different approximations. At higher shear rates ($\beta \geq 1$) the experimental data deviate from the theoretical predictions, but the results available are too sparse to provide a clear characterization of the behavior in this range of β. The assumption that chain properties depend on the chain length and on the shear rate only through the quantity β could also be questioned, since the chain relaxation time used to define β is the equilibrium one. In the high-β regime, theoretical considerations are more conjectural: various scaling pictures have been suggested for extremely high β values, such as the removal of EV effects in the scaling at fixed $\dot{\gamma}$[14,15] or the decoiling of a chain on the basis of the tensile blob model.[16]

Brownian dynamics (BD) techniques have also been used in the chain-in-flow context for models of a chain in continuous solvent similar to those treated theoretically.[17-20] Because the equations of motion are solved numerically in BD, models with HI, EV, and finite extensibility (rigid or finite extensible bonds) are obviously tractable: the whole range of β can be investigated, although the usefulness of this approach is limited by the low signal to noise ratio at small β and by possible limits to the validity of the model very far from equilibrium. As an example, BD results have

† Permanent address: Dipartimento di Fisica, Università degli Studi, Via Vetoio, Località Coppito, I-67100 l'Aquila, Italy. E-mail: cpierleo@sigrom.roma1.infn.it.

‡ E-mail: jryckaer@ulb.ac.be.

⊗ Abstract published in *Advance ACS Abstracts,* April 15, 1995.

0024-9297/95/2228-5097$09.00/0

confirmed the dependence on β^2 of the chain deformation mentioned above, but the data retain a quadratic dependence on β beyond $\beta = 1$, where experiments suggest a weaker dependence due to the finite extensibility of the real chains. Note also that when HI are considered, the BD method is rather demanding in computer time and has been restricted thus far to short chains ($N \leq 60$).[21]

Recently, equilibrium molecular dynamics (MD) has been used on a model of a chain in a fully atomic solvent at equilibrium.[22,23] Although only short chains could be studied, representative properties of dilute polymer solutions in good solvent conditions were obtained. For systems of 10−50 beads in liquid solvent, the expected scaling properties of the polymer size and internal structure (beyond the local structure) were reproduced. In addition, the longest relaxation time of the chain was found to scale as $\tau_N \sim N^{3\nu'}$, with $\nu' \leq \nu$ (ν is the Flory exponent for good solvent conditions), consistent with experimental findings.[24,25]

The present paper deals with simulations of a single chain in shear flow by nonequilibrium molecular dynamics (NEMD), i.e., on a fully microscopic level. We study short chains (10−50 beads) at a relatively high dilution and we are able to work at typical experimental reduced shear rates. Our results on the deformation and the orientation of the chain reproduce very satisfactorily all the available experimental data for chains in dilute solution undergoing shear flow. Furthermore, they suggest the existence of scaling laws for the chain sizes at fixed β in a reference frame defined on the basis of the principal axes of the average gyration tensor; this conclusion has been briefly reported elsewhere.[26] This is an important point since it allows one to predict the behavior of long chains used in the experiments from the results obtained for the relatively short chains of the simulation. The proposed scaling concerns both the global dimensions of the chain and its local correlations, with one β-dependent Flory exponent specific to each direction of the molecule-fixed frame. This provides a new coherent picture for the chain behavior in the intermediate regime of β. As a corollary, the deformation ratios frequently used to monitor the chain deformation induced by the flow are seen to be good N-independent quantities only at small β, i.e., so long as the scaling exponents retain their equilibrium values.

The paper is organized as follows: In section 2, we set up the essential phenomenology concerning a chain in shear flow and define the relevant structural characteristics of the chain. Section 3 deals with the microscopic model we have adopted: we also summarize the main results for the model at equilibrium. Technical details regarding the NEMD experiments are provided in section 4. Then, in section 5, we present results from the NEMD calculations, organized into two subsections: in section 5a, the scaling with N at fixed β is investigated, while in section 5b, we report results for various quantities for increasing reduced shear rate. Conclusions and perspectives are gathered together in the last section.

2. Phenomenological Framework

In this work we deal with simple shear flow characterized by the velocity field $\mathbf{u} = \dot{\gamma} y \mathbf{1}_x$ to which corresponds a velocity gradient κ with only one nonzero element $\kappa_{yx} = \dot{\gamma}$. Such a flow field can be regarded as the combination of a purely deformational flow, $\mathbf{u}_1 = (0.5\dot{\gamma} y \mathbf{1}_x + 0.5\dot{\gamma} x \mathbf{1}_y)$, and a purely rotational flow, $\mathbf{u}_2 = (0.5\dot{\gamma} y \mathbf{1}_x - 0.5\dot{\gamma} x \mathbf{1}_y)$, both taking place in the $x-y$ plane. In dilute solutions, the chain deformation and orientation under shear are measured by the anisotropy of tensorial quantities such as the gyration tensor $\mathbf{G}$, the end-to-end tensor $\mathbf{R}$, and the order parameter tensor $\mathbf{O}$, the latter being related, under suitable assumptions,[25,27] to the chain intrinsic birefringence. For a single chain of N beads, these tensors are defined in terms of the bead coordinates $\mathbf{r}_i$ ($i = 1, N$) as

$$\mathbf{G} = \frac{1}{2N^2} \sum_{i,j=1}^{N} \langle (\mathbf{r}_i - \mathbf{r}_j)(\mathbf{r}_i - \mathbf{r}_j) \rangle \tag{1}$$

$$\mathbf{R} = \langle (\mathbf{r}_1 - \mathbf{r}_N)(\mathbf{r}_1 - \mathbf{r}_N) \rangle \tag{2}$$

$$\mathbf{O} = \sum_{i=1}^{N-1} \left\langle \frac{(\mathbf{r}_{i+1} - \mathbf{r}_i)(\mathbf{r}_{i+1} - \mathbf{r}_i)}{(\mathbf{r}_{i+1} - \mathbf{r}_i)^2} - \frac{1}{3}\mathbf{1} \right\rangle \tag{3}$$

where $\langle ... \rangle$ indicates a statistical average. At equilibrium the system is isotropic and any of these three tensorial quantities, $\mathbf{A}$ say, is proportional to the unit tensor $\mathbf{1}$. In the shear flow geometry, symmetry considerations require that $A_{xz} = A_{zx} = A_{yz} = A_{zy} = 0$ at any shear rate. Hence there are at most four independent quantities to be monitored, namely, the three diagonal elements $A_{\alpha\alpha}$ ($\alpha = x, y, z$) and the off-diagonal element $A_{xy} = A_{yx}$. The orientational angle χ_A, defined through the relation

$$\cot(2\chi_A) = \frac{A_{xx} - A_{yy}}{2A_{xy}} \tag{4}$$

measures the rotation around $\mathbf{1}_z$ of the principal axes (I, II, III) of the tensor with respect to the flow frame (x, y, z). In shear flow, A_{xy} starts linearly with $\dot{\gamma}$ while the first contribution to $(A_{xx} - A_{yy})$ is of order $\dot{\gamma}^2$. Therefore the linear (Newtonian) regime is characterized by the value $\chi_A = \pi/4$. Outside the linear regime χ_A decreases to zero for increasing $\dot{\gamma}$. This behavior is qualitatively illustrated in Figure 1 for a 30-bead chain at two values of $\dot{\gamma}$.

The fundamental quantity for the investigation of the chain structure over the whole range of relevant length scales is the static structure factor defined as

$$S(\mathbf{k}) = \frac{1}{N} \sum_{i,j=1}^{N} \langle \exp[-\mathbf{k}\cdot(\mathbf{r}_i - \mathbf{r}_j)] \rangle \tag{5}$$

The low $k \equiv |\mathbf{k}|$ behavior is related to the gyration tensor, as can be easily seen from the series expansion

$$S(\mathbf{k}) = N[1 - \mathbf{k}\cdot\mathbf{G}\cdot\mathbf{k} + O(k^4)] \tag{6}$$

The intermediate-k regime gives direct information on the spatial correlation of monomers; at equilibrium, where the chain distribution is isotropic, the behaviour of $S(k)$ is dictated by certain scaling laws.[24,25]

As already mentioned in the Introduction, the physical parameter of importance in the study of the response of the system to shear flow is not the bare shear rate $\dot{\gamma}$ but the reduced shear rate, $\beta = \dot{\gamma}\tau_N$, where τ_N is the longest relaxation time of the polymer of N physical monomers. $\beta \ll 1$ is the regime of weak perturbation, since the chain is able to rearrange its configuration before the local strain has changed by a detectable amount, while $\beta \gg 1$ is the regime of strong perturba-

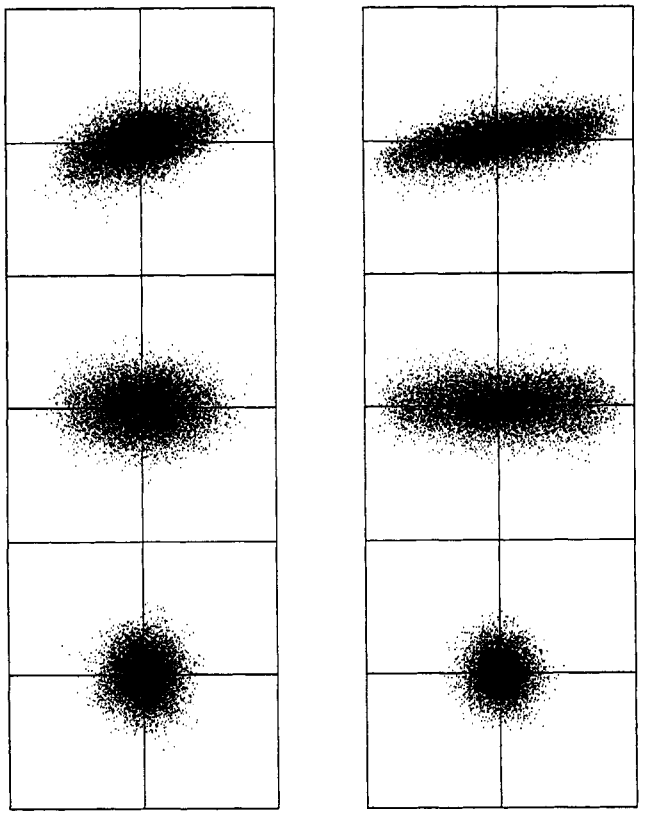

Figure 1. Shape and orientation of a 30-bead polymer under shear flow illustrated by projecting about 500 chain configurations on the three coordinate planes (xy, top; xz, middle; yz, bottom): (a) $\dot{\gamma} = 0.02126$ on the left; (b) $\dot{\gamma} = 0.0671$ on the right.

tions where the evolution of the chain structure is fully driven by the flow field. In real experiments τ_N is obtained through the relation

$$\tau_N = \frac{\eta_s[\eta]_0}{k_B T} \tag{7}$$

where k_B is the Boltzmann constant and T is the temperature; the Newtonian intrinsic viscosity $[\eta]_0$ of the solution and the solvent viscosity η_s are measurable quantities. With this definition the N dependence of β is given by the scaling behavior of the intrinsic viscosity (per chain), $[\eta]_0 \sim N^{3\nu'}$, where ν' is the apparent dynamic scaling exponent; $\nu' = 0.5$ in Θ-solvent and $\nu' \sim 0.55$ in good solvent conditions.[24,25]

3. Polymer in Solvent: Model and Equilibrium Properties

The microscopic model for the chain and the solvent[22,28] consists of a single linear chain of N beads of mass m connected by $N - 1$ rigid bonds of length d, embedded in N_s spherical solvent molecules with the same mass m as the polymer beads. The whole system occupies a cubic box of side L; either static or flow-adapted (Lee–Edwards[29]) periodic boundary conditions are applied to model bulk equilibrium or nonequilibrium situations, respectively.

All pair interactions between particles (either nonadjacent polymer beads or solvent particles) are represented by the same purely repulsive Lennard-Jones potential with energy and length parameters ϵ and σ.[30] Along the chain no restriction for the bond angles is explicitly considered other than the one arising from the pair repulsion between second-neighbor monomers. This model of *quasi-athermal* solvent corresponds to good solvent conditions for the polymer. Throughout this paper, all relevant quantities are expressed in units based on ϵ, σ, and m. In these units, the bond length between adjacent monomers is $d = 1.075$.

Table 1. Equilibrium Properties for the Simulated Chain Model[a]

N	R_g	$[\eta]_0$	$\tau_N = \eta_s[\eta]_0/k_BT$
9	1.53 ± 0.01	19 ± 1	22 ± 1
15	2.09 ± 0.02	44 ± 3	50 ± 3
20	2.50 ± 0.04	70 ± 5	80 ± 6
30	3.16 ± 0.03	132 ± 7	150 ± 8
50	4.26 ± 0.05	300 ± 24	342 ± 27

[a] N is the number of beads and R_g is the gyration ratio. Values of R_g for $N \leq 30$ are extracted by MD runs[20] while for $N = 50$ it is inferred by the scaling law given in the text (see section 3). The intrinsic viscosity per chain $[\eta]_0$ is computed as explained in the text (see the end of section 3). τ_N is the equilibrium relaxation time of the chain used in the definition of the reduced shear rate β.

All calculations, both at equilibrium and under shear conditions, were performed at a single state point defined by a temperature $k_BT/\epsilon = 1.5$ and an overall number density $\varrho = (N + N_s)/V = 0.8$, where k_B denotes the Boltzmann constant and V the volume of the system. Under these conditions, the linear viscosity of the pure solvent is $\eta_s = 1.71 \pm 0.01$.[31] The MD experiments were performed with constraint dynamics (SHAKE procedure[32]) using the velocity version of the Verlet algorithm as outlined in ref 28; the chosen time step was $\Delta t = 0.005$. As the simulated system is not infinite, it should be kept in mind that our calculations for one chain in solution could still be weakly dependent upon V (namely the amount of solvent surrounding the polymer). The role of finite size effects must therefore be addressed at each stage of the analysis.

Before focusing on chains in shear flow, we first summarize the main results obtained for the model at equilibrium.[22] Experiments were performed on chains of $N = 6$, 9, 20, and 30 beads; the volume of the box (and therefore the number of solvent molecules) was fixed in each case by requiring that the (expected) radius of gyration of the chain R_g never exceed 35% of the box length L. With this restriction imposed, we find that static properties are independent of box sizee (identical within the error bars). The scaling law $R_g = AN^\nu$ (with $A = 0.467 \pm 0.002$ and $\nu = 0.57 \pm 0.01$) is followed for short chains in continuous space; values of R_g are listed in Table 1. The chain structure factor $S(k)$ satisfies closely the universal behavior $S(k)/N = f(kR_g)$, as illustrated in Figure 2, while $S(k)$ behaves as $k^{-1/\nu}$ with $\nu = 0.58 \pm 0.01$ at high k and is almost independent of N: a perfect superposition of $S(k)$ at high k for the various N requires somewhat longer chains.[23] These results are important insofar as they define the reference equilibrium state against which the shear flow effects on the chain structure can be measured.

The dynamic properties of the chain at equilibrium are more complex, since dynamic scaling is not a true scaling for chains of finite length.[25] Moreover, in MD simulations with periodic boundary conditions, system-size effects on dynamic properties are unavoidable given the long-range nature of hydrodynamic interactions.[22,23] A detailed analysis of the finite-size effects, combined with a study of the chain length dependence, leads to the following picture:[22] at any fixed ratio R_g/L, the center-of-mass diffusion coefficient D scales as $D(L) =$

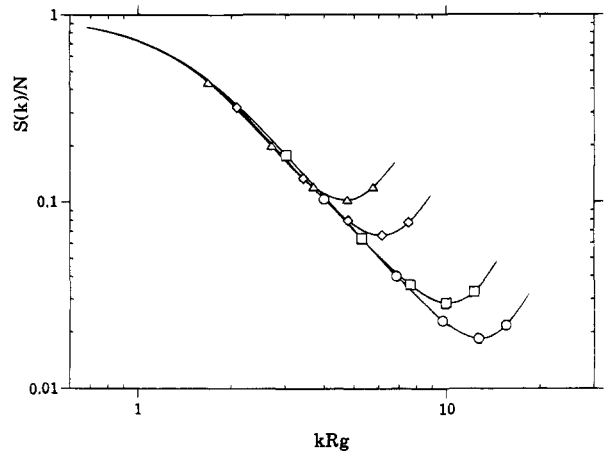

Figure 2. Universal equilibrium behavior of the normalized structure factor $S(k)/N$ versus kR_g for chain lengths $N = 6$ (triangles), 9 (diamonds), 20 (squares), and 30 (circles).

$G(R_g/L)N^{-\nu'}$ with an L-independent exponent. The MD results are found to be in very good agreement with the predictions of a generalized (L dependent) Kirkwood theory, which provides a way to extrapolate $G(R_g/L)$ to infinite dilution ($R_g/L = 0$).[22] The observed scaling in this limit is $D(\infty) = (0.120 \pm 0.002)N^{-\nu'}$ with $\nu' = 0.52 \pm 0.01$, to be compared with the experimental value $\nu' \sim 0.55$. This agreement for the scaling exponent shows that the MD simulation model reproduces correctly the EV and HI effects observed in real polymers in good solvents.

As already mentioned, in real experiments the longest relaxation time of the chain, τ_N, which enters in the definition of the reduced shear rate is usually estimated on the basis of the measured intrinsic viscosity of the solution. Given the noise level, the latter quantity is almost impossible to determine directly for our model system via (equilibrium) MD or NEMD simulation. In order to obtain τ_N we proceed indirectly through the use of the Einstein expression for the intrinsic viscosity, $[\eta]_0 = 10/3\pi R_h^3$, where it is assumed that the polymer behaves as a rigid sphere with a hydrodynamic radius R_h.[24] We fix the last quantity through Stokes' law, $R_h = k_BT/(6\pi\eta_s D(\infty))$, where all factors on the right-hand side are derived from the simulations. We stress that in this way the definition used for the reduced shear rate in the NEMD experiments is independent of the box size. Such a choice is supported by empirical observation: simulation of a 9-bead chain in two different boxes, corresponding to $R_g(\text{eq})/L = 0.24$ and $R_g(\text{eq})/L = 0.14$, at the same shear rate $\dot\gamma = 0.2$ provides indistinguishable results (within error bars) for all the static properties of the chain we consider in this work (see results of run 9J of section 5). Further support to this system size independence is given by the absence of system-size effects in the equilibrium time correlation functions related, through the fluctuation–dissipation theorem, to the orientation and the deformation of the chain at vanishing shear rate.[33]

4. Simulation of a Chain in Simple Shear Flow

In the NEMD simulations, the shear flow $\mathbf{u} = \dot\gamma y \mathbf{1}_x$ is produced by the molecular version of the so-called SLLOD equations.[34] Planar Couette flow is set up at $t = 0$ (equilibrium situation) and maintained homogeneously in space and constant in time at later times. We summarize here the procedure required to sample the stationary nonequilibrium situation to which the system evolves. In practice, for each selected equilibrium configuration of the $(N + N_s)$ particles, the instantaneous velocities of the polymer beads and the solvent molecules are augmented by a systematic component $\Delta\mathbf{v} = \dot\gamma y \mathbf{1}_x$, where y is the corresponding polymer or the solvent molecule center-of-mass coordinate. The homogeneous flow can be maintained indefinitely by use of Lees–Edwards boundary conditions;[29] the heat continuously dissipated within the system as a result of the imposed gradient is removed by coupling the system to a Nosé–Hoover thermostat.[35] The equations of motion describing the evolution of the system are as follows. For the solvent molecules with coordinates $\mathbf{r}_i$ and linear momenta $\mathbf{p}_i$ ($i = 1, N_s$), one has

$$\dot{\mathbf{r}}_i = \frac{\mathbf{p}_i}{m} + \theta(t)\kappa^T\cdot\mathbf{r}_i \tag{8a}$$

$$\dot{\mathbf{p}}_i = \mathbf{F}_i - \theta(t)\kappa^T\cdot\mathbf{r}_i - \nu_N\xi\mathbf{p}_i \tag{8b}$$

and for the polymer beads with coordinates $\mathbf{r}_k$ and linear momenta $\mathbf{p}_k$ ($k = 1, N$)

$$\dot{\mathbf{r}}_k = \frac{\mathbf{p}_k}{m} + \theta(t)\kappa^T\cdot\mathbf{R} \tag{9a}$$

$$\dot{\mathbf{p}}_k = \mathbf{F}_k + \mathbf{G}_k - \theta(t)\kappa^T\cdot\mathbf{P} - \nu_N\xi\mathbf{p}_k \tag{9b}$$

$\mathbf{R}$ and $\mathbf{P}$ are, respectively, the coordinates and the momentum of the polymer center of mass; $\mathbf{F}_k$ (or $\mathbf{F}_i$) is the total force on a polymer bead (or a solvent molecule) deriving from the interparticle potential; $\mathbf{G}_k$ is the sum of the constraint forces (directed along the bonds involving the bead) acting on bead k; and $\xi(t)$ is an extra variable playing the role of a time-dependent friction coefficient, the time evolution of which is given by

$$\dot\xi = \nu_N\left[\frac{2K_G}{gk_BT} - 1\right] \tag{10}$$

where K_G is the instantaneous total kinetic energy of all molecules in the system (see below), g is the number of independent degrees of freedom, namely $g = (3N_s + 2N - 2)$, ν_N is a parameter monitoring the strength of the coupling with the heat bath (thermalization rate), and the step function $\theta(t)$ indicates that the external field is turned on at $t = 0$. Equations 8 and 9 can be rewritten as second-order differential equations:

$$\ddot{\mathbf{r}}_i = \frac{\mathbf{F}_i}{m} + \kappa^T\cdot\mathbf{r}_i\delta(t) - \nu_N\xi(t)[\dot{\mathbf{r}}_i - \theta(t)\kappa^T\cdot\mathbf{r}_i] \tag{11a}$$

$$\ddot{\mathbf{r}}_k = \frac{\mathbf{F}_k + \mathbf{G}_k}{m} + \kappa^T\cdot\mathbf{R}\delta(t) - \nu_N\xi(t)[\dot{\mathbf{r}}_k - \theta(t)\kappa^T\cdot\mathbf{r}_k] \tag{11b}$$

The first term on the right-hand side of eqs 11 is the usual acceleration due to the interparticle forces. The second term is the instantaneous acceleration that must be applied at time $t = 0$ in order to initialize the required velocity field, $\mathbf{v}(\mathbf{r},t) = \theta(t)\kappa^T\cdot\mathbf{r}$, in the system. The last term is the contribution from the Nosé–Hoover thermostat. Note that for an arbitrary homogeneous flow with curved flow lines, an additional term appears.[36] The dynamics of the Nosé variable (eq 10) is controlled by the kinetic energy, which involves the thermal part

Table 2. List of Experiments and Simulation Details[a]

expt	N	N_s	$\dot{\gamma}$	β	L/b	τ
9A	9	207	0.002	0.043 ± 0.003	6	200 × 75
9B	9	207	0.02	0.43 ± 0.03	6	200 × 75
9C	9	207	0.02	0.43 ± 0.03	6	10000
9D	9	207	0.035	0.76 ± 0.04	6	1000
9E	9	207	0.05	1.08 ± 0.06	6	5000
9F	9	207	0.072	1.6 ± 0.1	6	15000
9G	9	207	0.0926	2.0 ± 0.1	6	15000
9H	9	207	0.139	3.1 ± 0.2	6	15000
9I	9	207	0.2	4.3 ± 0.3	6	200 × 75
9J	9	207	0.2	4.3 ± 0.3	10	5000
9K	9	207	1	19 ± 1	6	100 × 75
9L	9	207	1	19 ± 1	6	5000
20A	20	980	0.0207	1.7 ± 0.1	10	20000
20B	20	980	0.04	3.2 ± 0.2	10	2000
20C	20	980	0.2385	19 ± 1	10	5000
30A	30	2167	0.011	1.65 ± 0.09	13	50000
30B	30	2167	0.02126	3.2 ± 0.2	13	25000
30C	30	2167	0.0671	10.0 ± 0.5	13	25000
30D	30	2167	0.5	75 ± 4	13	25000
50A	50	4046	0.00958	3.3 ± 0.3	16	25000

[a] N is the number of beads in the chain, N_s is the number of solvent particles, $\dot{\gamma}$ is the shear rate, and β is the reduced shear rate as defined in the text. The box size is indicated by its side L and b is the bond length. τ indicates the time length of the run in units τ_{LJ} for stationary NEMD, or the number of segments times the length of each segment in units τ_{LJ} for dynamical NEMD.

of the velocity, namely

$$K_G = \frac{m}{2}\sum_i (\dot{\mathbf{r}}_i - \theta(t)\kappa^T\cdot\mathbf{r}_i)^2 \qquad (12)$$

where the sum runs over both solvent and monomer particles.

The algorithm used to integrate eqs 10 and 11 is an extension of the one used for the equilibrium MD calculations on the same system, mentioned in the previous section. As particle accelerations are now dependent on their velocities, a prediction followed by a short iteration loop needs to be done in order to integrate the velocities.[28] In the present work, the Nosé thermostating rate was fixed at $\nu_N = 8.67$.

The NEMD experiments can be conducted by two different procedures. One possibility is to follow for a time $t > \tau_N$ the transient behavior of the system, initially at equilibrium, toward the stationary state characterized by the homogeneous shear flow (*dynamical method*). Alternatively one can generate a single trajectory for a very long time $t \gg \tau_N$ in order to probe the nonequilibrium steady state itself (*stationary* method). Both procedures require the use of eq 11; the first method consists in averaging over many initial equilibrium configurations the response of the system to the imposed shear flow set up at time $t = 0$, while in the second method statistical averages are replaced by time averages through the ergodic hypothesis.[36] Here we have mainly followed the stationary method, which is somewhat cheaper in terms of computer time. Only a few runs were performed by the dynamical method.

5. Simulation Results

In the present study we spanned the range of $\dot{\gamma}$ between 0.002 and 1. The onset of non-Newtonian behavior in the pure solvent, detected as a shear thinning, arises around $\dot{\gamma} = 0.5$.[31] We simulated chains of four lengths, $N = 9$, 20, 30, and 50, in $N_s = 207$, 980, 2167, and 4046 solvent particles, respectively, covering reduced shear rates in the range $0.4 \le \beta \le 75$. For each chain length the size of the system is chosen in a way to work at $R_g/L \simeq 0.24$. Details of the experiments are listed in Table 2, while in Tables 3 and 4 we collect the results for G_α, R_α (α = I, II, III), χ_G, and χ_R. For the order parameter tensor we report the *amount of birefringence* $\Delta O = O_I - O_{II} = [(O_{xx} - O_{yy})^2 + 4O_{xy}^2]^{1/2}$, the *second normal polarizability difference* $(O_{zz} - O_{yy})$, and the *extinction angle* χ_O defined by eq 4 (note that (i) the traceless tensor **O** is completely characterized by three independent quantities in shear flow geometry and (ii) **O** is only proportional to the polarizability tensor of the system,[25] and therefore only the extinction angle can be compared with experimental data).

Our results are presented in two successive subsections. First we investigate the existence of possible scaling laws for the chain dimensions at fixed β, namely the self-similar character of chain configurations corresponding to chains of increasing length N subjected to shear flow with related decreasing absolute shear rates. Then we study the β-dependence of the various quantities related to the chain structure.

A. Scaling at Fixed β. A key quantity for monitoring the scaling behavior of a polymer is the chain structure factor. At equilibrium the gyration ratio R_g can be extracted from the small-k behavior of $S(k)$ ($kR_g \ll 1$) (see eq 6) and, provided the chain is sufficiently long for $S(k)$ to become N independent at large k, a power law behavior $S(k) \sim k^{-1/\nu}$ holds in the range $2.5/R_g \le k \le \pi/d$, where ν is the static scaling exponent. Similarly, the chain center-of-mass diffusion coefficient

Table 3. Orientation Angle χ_G, Eigenvalues of the Gyration Tensor G, and Scaling Exponents in Directions I, II, and III As Inferred by the High-k Behavior of the Structure Factor $S(k)$

β	expt	$\cot(2\chi_G)$	G_I	G_{II}	G_{III}	ν_I	ν_{II}	ν_{III}
0.043 ± 0.003	9A		0.78 ± 0.03	0.77 ± 0.03	0.74 ± 0.03			
0.43 ± 0.03	9C		0.85 ± 0.04	0.68 ± 0.03	0.77 ± 0.05	0.58 ± 0.01	0.53 ± 0.02	0.56 ± 0.02
0.76 ± 0.04	9D	0.4 ± 0.1	1.01 ± 0.04	0.63 ± 0.03	0.73 ± 0.03	0.62 ± 0.03	0.54 ± 0.03	0.54 ± 0.02
1.08 ± 0.06	9E	0.6 ± 0.1	1.11 ± 0.05	0.57 ± 0.02	0.73 ± 0.03	0.63 ± 0.02	0.52 ± 0.03	0.57 ± 0.02
1.6 ± 0.1	9F	0.86 ± 0.08	1.19 ± 0.04	0.52 ± 0.01	0.74 ± 0.03	0.66 ± 0.02	0.51 ± 0.03	0.56 ± 0.02
1.7 ± 0.1	20A	0.87 ± 0.15	3.7 ± 0.2	1.42 ± 0.04	1.9 ± 0.1	0.68 ± 0.02	0.52 ± 0.02	0.56 ± 0.02
1.65 ± 0.09	30A	0.9 ± 0.1	6.6 ± 0.3	2.28 ± 0.08	3.17 ± 0.15	0.67 ± 0.01	0.52 ± 0.01	0.56 ± 0.02
2.0 ± 0.1	9G	0.97 ± 0.09	1.32 ± 0.04	0.51 ± 0.01	0.70 ± 0.02	0.66 ± 0.02	0.51 ± 0.03	0.57 ± 0.02
* 3.1 ± 0.2	9H	1.28 ± 0.07	1.50 ± 0.03	0.46 ± 0.01	0.66 ± 0.02	0.67 ± 0.02		0.57 ± 0.02
* 3.2 ± 0.2	20B	1.4 ± 0.1	5.1 ± 0.2	1.15 ± 0.03	1.8 ± 0.1	0.70 ± 0.01	0.48 ± 0.01	0.54 ± 0.02
* 3.2 ± 0.2	30B	1.5 ± 0.2	8.7 ± 0.5	1.8 ± 0.1	3.1 ± 0.3	0.69 ± 0.01	0.48 ± 0.01	0.54 ± 0.02
* 3.3 ± 0.2	50A	1.5 ± 0.7	17 ± 2	3.2 ± 0.1	5.3 ± 0.5	0.69 ± 0.01	0.49 ± 0.01	0.54 ± 0.02
4.3 ± 0.3	9J	1.4 ± 0.2	1.67 ± 0.07	0.40 ± 0.01	0.64 ± 0.03	0.66 ± 0.02		0.57 ± 0.02
10.0 ± 0.5	30C	2.97 ± 0.29	21 ± 1	1.25 ± 0.06	2.0 ± 0.2	0.76 ± 0.04	0.45 ± 0.02	0.53 ± 0.02
19 ± 1	9L	3.4 ± 0.1	2.98 ± 0.05	0.22 ± 0.004	0.42 ± 0.01	0.66 ± 0.02		
19 ± 1	20C	3.5 ± 0.4	11.5 ± 0.9	0.61 ± 0.03	1.3 ± 0.1	0.71 ± 0.03	0.46 ± 0.05	
75 ± 4	30D	7.6 ± 0.3	41 ± 1	0.46 ± 0.01	1.2 ± 0.1	0.72 ± 0.02		

Table 4. Extinction Angle χ_O, Orientation Angle χ_R, Amount of Birefringence ΔO, Second Normal Polarizability Difference $O_{zz} - O_{yy}$, and the Eigenvalues of the End-to-End Tensor R

β	expt	$\cot(2\chi_O)$	$\cot(2\chi_R)$	ΔO	$O_{zz} - O_{yy}$	R_I	R_{II}	R_{III}
0.043 ± 0.003	9A					4.6 ± 0.3	4.5 ± 0.3	4.6 ± 0.3
0.43 ± 0.03	9C		0.08 ± 0.12	0.17 ± 0.02		5.4 ± 0.3	3.6 ± 0.3	4.6 ± 0.1
0.76 ± 0.04	9D	0.3 ± 0.1	0.35 ± 0.1	0.31 ± 0.04		6.7 ± 0.3	3.5 ± 0.2	3.9 ± 0.4
1.08 ± 0.06	9E	0.4 ± 0.1	0.8 ± 0.2	0.47 ± 0.02		7.4 ± 0.5	3.1 ± 0.2	4.3 ± 0.3
1.6 ± 0.1	9F	0.47 ± 0.05	1.0 ± 0.1	0.54 ± 0.02	0.05 ± 0.02	8.1 ± 0.4	2.7 ± 0.1	4.4 ± 0.3
1.7 ± 0.1	20A	0.42 ± 0.06	1.0 ± 0.2	0.71 ± 0.07		27 ± 2	7.6 ± 0.3	11 ± 1
1.65 ± 0.09	30A	0.49 ± 0.05	1.0 ± 0.2	0.86 ± 0.05		49 ± 3	12.8 ± 0.8	21 ± 1
2.0 ± 0.1	9G	0.53 ± 0.05	1.1 ± 0.1	0.67 ± 0.03	0.03 ± 0.02	9.3 ± 0.4	2.56 ± 0.07	4.1 ± 0.2
* 3.1 ± 0.2	9H	0.69 ± 0.03	1.3 ± 0.1	0.94 ± 003	0.04 ± 0.02	10.8 ± 0.3	2.37 ± 0.07	3.9 ± 0.2
* 3.2 ± 0.2	20B	0.70 ± 0.04	1.5 ± 0.2	1.33 ± 0.05	0.05 ± 0.03	40 ± 2	6.4 ± 0.4	12 ± 1
* 3.2 ± 0.2	30B	0.78 ± 0.08	1.7 ± 0.2	1.5 ± 0.1	0.08 ± 0.07	67 ± 4	9.4 ± 0.8	19 ± 3
* 3.3 ± 0.2	50A	0.7 ± 0.1	2.0 ± 0.7	1.7 ± 0.2		132 ± 25	17 ± 1	34 ± 4
4.3 ± 0.3	9J	0.75 ± 0.06	1.6 ± 0.2	1.22 ± 0.05	0.12 ± 0.04	12.2 ± 0.7	1.91 ± 0.07	4.2 ± 0.4
10.0 ± 0.5	30C	1.6 ± 0.1	3.3 ± 0.4	4.7 ± 0.3	0.08 ± 0.13	180 ± 14	6.8 ± 0.2	12 ± 1
19 ± 1	9L	1.82 ± 0.03	3.9 ± 0.2	3.16 ± 0.04	0.27 ± 0.02	23.4 ± 0.6	1.04 ± 0.04	2.3 ± 0.2
19 ± 1	20C	1.7 ± 0.1	4.4 ± 0.6	5.0 ± 0.2	0.2 ± 0.1	97 ± 6	2.7 ± 0.1	8.9 ± 0.8
75 ± 4	30D	3.39 ± 0.06	10.0 ± 0.6	14.2 ± 0.3	0.38 ± 0.15	353 ± 13	2.36 ± 0.02	8 ± 1

and the dynamic scaling exponent can be extracted from the "small"-k and "high"-k behavior, respectively, of the dynamic structure factor.[22] The static scaling analysis for the equilibrium situation is based on the assumption that there exists an underlying scaling transformation $N \to N/\lambda$, $d \to d\lambda^{\nu}$ which leaves R_g invariant ($R_g \sim dN^{\nu}$): it then uses dimensional analysis to extract the high-k behavior of $S(k)$. It is therefore natural to investigate the possible extension of the scaling analysis to the present anisotropic situation, where the chain is deformed by the shear flow.

Theoretical predictions indicate that under shear flow at the same reduced shear rate β, chains of different length N are oriented at the same angle χ_G with respect to the flow. Such a prediction, which was partially confirmed by early experiments,[3] is found to be in agreement with our results (see Tables 3 and 4 and the discussion in the next subsection). This "universal" dependence of χ_G on the relevant nonequilibrium parameter β suggests an investigation of scaling for chain dimensions in the molecular reference frame at fixed β. We did so in considering four chain lengths $N = 9$, 20, 30, and 50 at fixed $\beta = 3.2$ Results of such simulations are indicated by an asterisk in Tables 3 and 4.

At equilibrium the existence of scaling transformation implies that the chain normalized structure factor is a universal function $S(k)/N = f(kR_g)$ up to $k \approx 2\pi/d$, above which the local structure of the chain appears. The $k^{-1/\nu}$ power law (see above) for $S(k)$ at high k then follows from the expected N-independence of the structure factor when spatial correlations are probed over length scales smaller than R_g. A similar universality is observed for chains in shear flow in the case where **k** is oriented along the principal axes of the gyration tensor (α = I, II, III): $S(k_\alpha)/N = f_\alpha(k_\alpha G_\alpha^{1/2})$ up to $k_\alpha \approx 2\pi/d$. This is illustrated in Figure 3 for directions I and II; results for direction III are not shown since they do not differ significantly from the equilibrium behavior (see Figure 2). In the high-k region, the N-independence of $S(k_\alpha)$ is indeed observed in directions I and III, but not in direction II, as shown in Figure 4. We believe that the residual N-dependence is related to the smaller dimension of the chains in the compression direction II. However, it is already clear from Figure 3 that $S(k)$ for each chain length and in each direction follows the "long"-chain behavior $S(k_\alpha) \sim k^{-1/\nu_\alpha}$ above $k_\alpha = 1.5/G_\alpha^{1/2}$. Estimates of ν_I, ν_{II}, and ν_{III} on the basis of $S(k_\alpha)$ power laws are given in Table 3. At the same β value, G_I, G_{II}, and G_{III} are compatible with power law behaviors $G_\alpha \sim (N-1)^{2\nu_\alpha}$ (see Figure 5), from which we obtain the estimates $\nu_I = 0.69 \pm 0.02$, $\nu_{II} = 0.53 \pm 0.03$, and $\nu_{III} = 0.58 \pm 0.03$. The observed agreement between high- and low-k estimates of scaling exponents strongly supports an anisotropic scaling picture with β-dependent exponents.

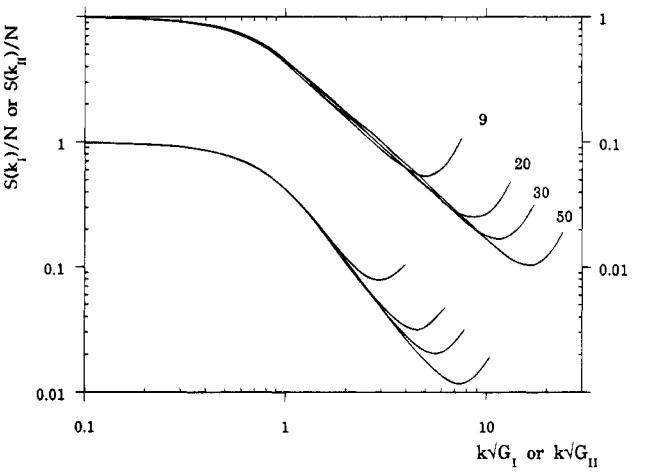

Figure 3. $\beta = 3.2$. Universal behaviors for the normalized structure factor $f(k_\alpha G_\alpha^{1/2}) = S(k_\alpha)/N$ versus $k_\alpha G_\alpha^{1/2}$ for α = I (upper curves) and α = II (lower curves) and for all chain lengths.

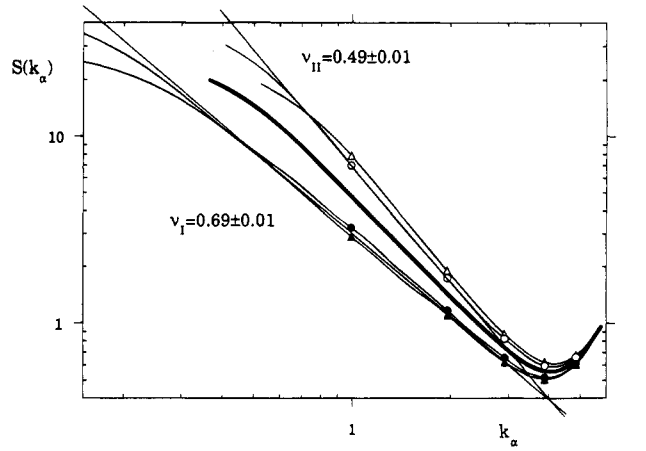

Figure 4. $\beta = 3.2$. $S(k_\alpha)$ versus k_α for α = I (filled symbols) and α = II (open symbols) for $N = 30$ (triangles) and $N = 50$ (circles). The thick line is the equilibrium behavior for $N = 30$. $S(k)$ along III (not indicated on the figure for the sake of clarity) remains close to equilibrium.

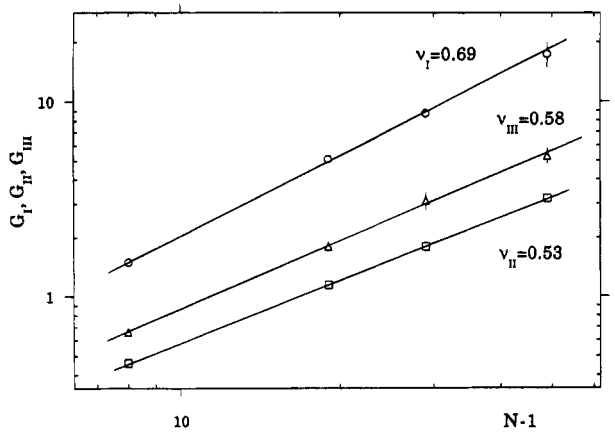

Figure 5. $\beta = 3.2$. Scaling behavior for the eigenvalues of the gyration tensor G_I (circles), G_{II} (squares), and G_{III} (triangles) versus $(N - 1)$. Estimates of the scaling exponents ν_α (α = I, II, III) obtained by fitting the data with the laws $G_\alpha \sim (N - 1)^{2\nu_\alpha}$ are indicated.

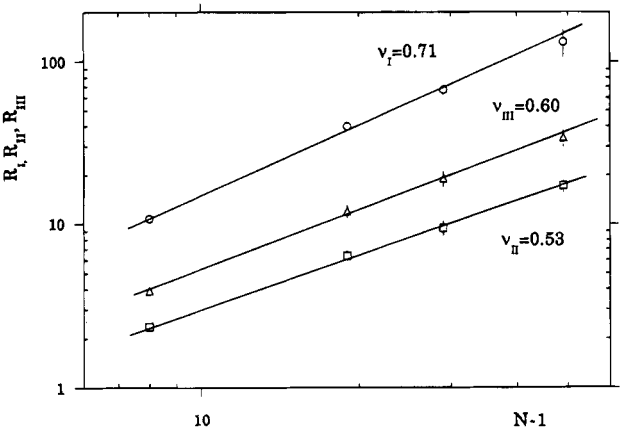

Figure 6. $\beta = 3.2$. Scaling behavior for the eigenvalues of the end-to-end tensor R_I (circles), R_{II} (squares), and R_{III} (triangles) versus $(N - 1)$. Estimates of the scaling exponents ν_α (α = I, II, III) obtained by fitting the data with the laws $R_\alpha \sim (N - 1)^{2\nu_\alpha}$ are indicated.

At equilibrium, the end-to-end distance and the gyration radius are known to follow the same scaling law. In shear flow at fixed β, the gyration tensor and the end-to-end tensor appear to be oriented in the same way, within error bars (see Tables 3 and 4). Figure 6 shows that the eigenvalues of the end-to-end tensor (R_α, α = I, II, III) follow $(N - 1)^{2\nu_\alpha}$ power laws with exponents in agreement with those obtained for the gyration tensor.

The above scaling picture for chains in shear flow is consistent with the available SANS data for polystyrene in dilute solution in good solvent conditions.[2] Figure 5 of ref 2b reports measurements of $S(k_x)$ and $S(k_z)$ for a chain of molecular mass $M_w = 2.8 \times 10^5$ g mol^{-1} in shear flow at $\beta = 3.17$. At such a β value, $S(k_x)$ and $S(k_I)$ are essentially identical, as illustrated in Figure 7 for the case $N = 30$. Assuming that the same holds for the experimental case, we infer from the SANS data that $\nu_I \sim 0.7$, in remarkable agreement with the value obtained from MD. It is unfortunate that experiments on chains of different lengths at a fixed value of β have not been performed so far. A more complete test of our scaling picture obviously requires further experimental investigations.

Having established a scaling property for the shear flow deformed polymer structure on the basis of "short"-chain simulations in combination with $S(k)$ data for real

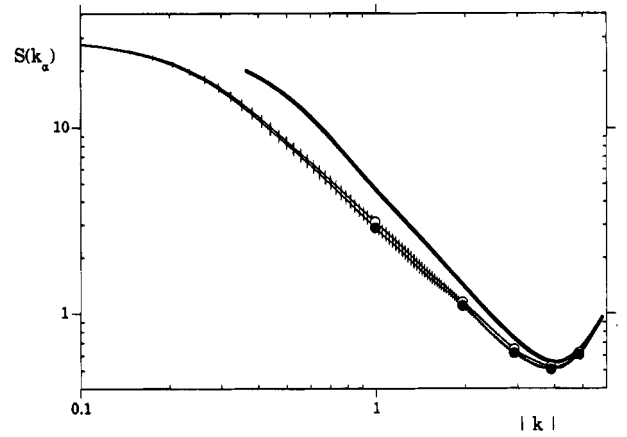

Figure 7. $\beta = 3.2$. Comparison between $S(\mathbf{k})$ for $\mathbf{k}$ along the flow direction (x-axis, open circles) and $S(\mathbf{k})$ for $\mathbf{k}$ along the extension direction (I-axis, filled circles) for $N = 30$. The thick line represents the equilibrium behavior.

polymers, a natural question arises: what is the gap between the polymer size chosen in MD and that used in real experiments? In fact, the chain used in the neutron scattering experiment at high k^2 appears to be only 3–4 times longer than the largest polymer size considered here ($N = 50$). The size of a flexible chain can be expressed as the number of effective "independent" monomers N_{eff}, a number which is obtained by dividing the chain contour length by the persistence length $l \equiv 2\pi/k_m$, where k_m is the k-value at which the power law $k^{-1/\nu}$ ceases to be observed in the $S(k)$, that is, the k value above which the local structure of the chain becomes manifest. Our chain of $N = 50$ beads corresponds to $N_{eff} = 27$ ($L_c = 54$ and $l = 2$; see Figure 4). If we now apply the same criteria to the polystyrene chain in ref 2, we obtain $N_{eff} = 100$ with a contour length $L_c = 625$ nm (obtained from the polymer weight $M_w = 2.8 \times 10^5$ g mol^{-1}, the single chemical unit weight $m_w = 112$ g mol^{-1}, and the length of the single chemical unit of 0.25 nm) and a persistence length of about $l = 2\pi$ nm. Moreover, in our model solvent particles have the same size as chain beads and with the above criterion, this would correspond to solvent molecules of 3 nm diameter, that is, a factor 3–5 times larger than ordinary solvents.

B. β-Dependence of the Results. In this section we discuss the shear-rate dependence of various indicators of the orientation and deformation of chains of different lengths N. The general picture emerging from theoretical models for a chain in shear flow is that (i) the orientation angle of any tensor **A** associated with the chain structure follows the behavior

$$\cot(2\chi_A) = \frac{\beta}{m_A} \tag{13}$$

where m_A is a universal constant, and (ii) the relative deviation from equilibrium of the diagonal elements $G_{\alpha\alpha}$ ($\alpha = x, y, z$) of the gyration tensor, $\delta_{\alpha\alpha} = [G_{\alpha\alpha}(\beta) - G_{\alpha\alpha}(0)]/G_{\alpha\alpha}(0)$, follows the behavior

$$\delta_{\alpha\alpha} = C_\alpha \beta^2 \tag{14}$$

where C_α is also a universal constant. As a consequence, the nonequilibrium deviation of the trace of **G** also exhibits a β^2 behavior. Exact values for m_O, m_G, m_R, and C_α can be obtained only for the simplest Rouse model,[6,7] while the model with EV and/or HI in their

Table 5. Theoretical Results for Chain Orientation and Deformation[a]

EV	no	no	yes	yes	no	no
HI	no	preav	no	preav	yes	yes
FE	no	no	no	no	no	no
C_x	0.457	0.185			0.29	0.27
C_y	0.0	0.0			~0.0	-6.9×10^{-3}
C_z	0.0	0.0			~0.0	0.0
C	0.152	0.062	0.231	0.16	0.12 ± 0.02	0.09
m_G	1.75	2.83				
C_R	0.2	0.08	0.262	0.18		
m_R	1.67	2.67				
C_O					0.68 ± 0.05	
m_O	2.5	4.88			3.4 ± 0.2	
refs	6, 7	6, 7	7	7	19, 20	11

preaveraged form can be solved by the approximate classical Zimm procedure.[7,25] Another model of the chain dynamics in solvent, based on a system of coupled Langevin equations for the chain degrees of freedom and the solvent local hydrodynamic variables, has been extensively studied by renormalization group theory techniques at equilibrium[37] and in elongational or shear flows.[8-14,38] For a chain in shear flow this approach predicts an expansion of the chain along the x axis, a very minor contraction along the y axis, and no change in the z direction.[11] For clarity, we collect in Table 5 the theoretical predictions of the various models together with the results of recent BD simulations.[19,20]

The law (14) is in contradiction with the anisotropic scaling behavior of the previous section. Indeed, at $\beta = 3.2$, since the chain has scaling exponents in the principal-axis directions which differ from the equilibrium one, the coefficients C_α ($\alpha = x, y$) introduced in eq 14 cannot be N-independent: instead they should present a smooth N-dependence which eventually will follow the scaling law $N^{(\nu_I(\beta)-\nu_{eq})}$ in the $N \to \infty$ limit. Note that the same picture also holds for the trace of the gyration and the end-to-end tensors. The contradiction is only an apparent one if we consider the limits of applicability of the theoretical models. The latter are all based on the Rouse harmonic bond connectors (or Edwards Hamiltonian in the continuum limit) which cannot account for the finite extensibility of real chains. Moreover, the inclusion of HI in the preaveraged form is only justified in the region of small β while a full treatment of HI avoiding preaveraging requires a self-consistent procedure which is difficult to handle.[11,13] The theoretical laws (13) and (14) are therefore expected to describe the orientation and deformation of real chains only at small β values ($\beta < 1$), a regime where it is observed (see below) that shear flow influences the power law for G_α at the prefactor level but maintains the scaling exponents at their equilibrium values.

We now analyze our results in a systematic way and compare them with experimental data and theoretical predictions.

The effective coefficients m_G and m_O, computed according to their definition in eq 13, are presented for increasing β in Figure 8 for all chain lengths investigated. First, we note that chains of different length but considered at the same β value are equally oriented (within error bars). We observe moreover that $m_O \geq m_G$ at any β; i.e., **G** is more easily oriented than **O**. The end-to-end tensor is always oriented like **G**, as can be inferred from Tables 3 and 4. We finally note that both m_O and m_G increase with β, indicating a saturation effect on the orientation of the chain. In Figure 8 we also show the fitted curve $m_G = (2.1 + 0.1\beta)$ for $0 \leq \beta \leq 12$, which has been recently inferred from light scattering (LS) data for polystyrene ($M_w = 10.3 \times 10^6$ g mol^{-1}) in dioctyl phthalate at the Θ-point. The very good agreement observed between our data and the experimental fit confirms that m_G is an N-independent quantity in this range of β (or at least its N-dependence is very weak). It also suggests that EV effects (present in simulations but absent in the present experiments) are of minor importance for the chain orientation. Because of the large error bars on our data at small β, it is difficult to draw definite conclusions about the link with the various theoretical predictions of Table 5. The only clear indication is that the value $m_O = 4.88$ for the case with preaveraged HI is in worse agreement than the estimates for the nonpreavereged case ($m_O = 3.4 \pm 0.2$) and the ideal chain (no HI) case ($m_O = 2.5$).

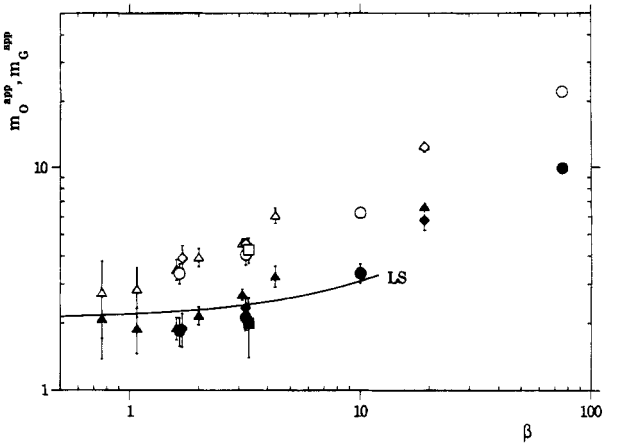

Figure 8. Effective coefficients $m_O^{app} = \beta/\cot(2\chi_O)$ (open symbols) and $m_G^{app} = \beta/\cot(2\chi_G)$ (filled symbols) versus β for various chain lengths: $N = 9$ (triangles), $N = 20$ (diamonds), $N = 30$ (circles), and $N = 50$ (squares). The law $m_G^{app} = (2.1 + 0.1\beta)$ fitted to light scattering data[4] in the range $0 \leq \beta \leq 12$ is indicated by LS.

Coming back to our scaling analysis, we now investigate the β-dependence of the various scaling exponents ν_α (α = I, II, III). This can be most easily inferred from the intermediate-k regime of $S(k_\alpha)$. In Figure 9 we show $S(\mathbf{k})$ for $\mathbf{k}$ along the three principal axes of the gyration tensor for a 30-bead chain at $\beta = 0$, 1.65, 10, and 75. The figure reveals clearly the general trend of the exponents; up to $\beta = 10$ at least, ν_I increases with β, ν_{II} decreases with increasing β, and ν_{III} remains practically equal to the equilibrium value. However, for $\beta = 75$, the trends seem to invert: a close look at the curves of $S(k_\alpha)$ suggests a saturation effect due to the finite length of the chain. Indeed, at such a value of β, even the local chain structure at the monomer length scale is strongly deformed in the three directions and therefore the $S(k)$ loses its universal character and becomes strongly N-dependent. Note that $\beta = 75$ for $N = 30$ corresponds to $\dot{\gamma} = 0.5$. which in turn corresponds to the onset of non-Newtonian behavior for the solvent.[31] For the sake of clarity, let us call the saturation effect arising from the finite length of the chain the *finite chain saturation* effect (FCS). It is clear that the shorter the chain is, the sooner FCS will appear as β increases. We estimate that for the present model at the thermodynamic point considered in this study, the onset of FCS occurs for $\dot{\gamma} \sim 0.1$. This fact probably explains why the data for $N = 9$ in Figure 8 deviate slightly from the data for longer chains for $\beta > 2$.

In Figure 10 we show the variation with β of the exponents ν_I and ν_{II} as inferred from the intermediate-k region of the structure factor (see Table 3). For each exponent, values obtained for different N fall on a

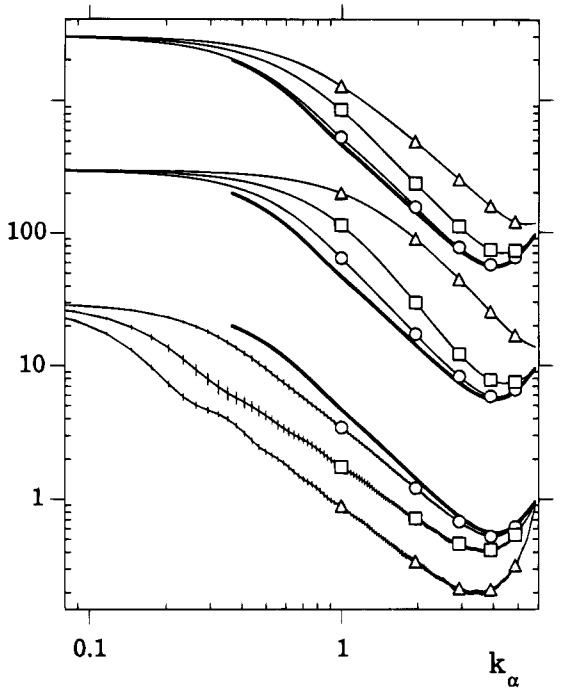

Figure 9. $N = 30$. Evolution of $S(\mathbf{k})$ with β for $\mathbf{k}$ along the principal axes of the gyration tensor: I (bottom), II (middle), and III (top). Four β values are shown: $\beta = 0$ (thick lines), $\beta = 1.65$ (circles), $\beta = 10$ (squares), and $\beta = 75$ (triangles).

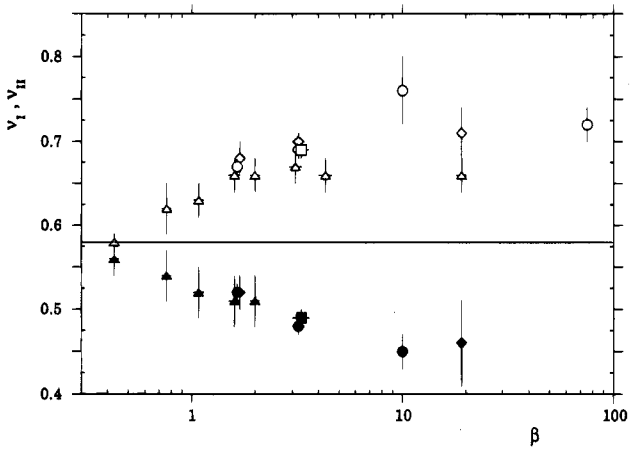

Figure 10. Evolution with β of the scaling exponents ν_I (open symbols) and ν_{II} (filled symbols) as inferred by the high-k behavior of the structure factor. $N = 9$ (triangles), $N = 20$ (diamond), $N = 30$ (circles), and $N = 50$ (squares). The equilibrium value is indicated by the horizontal line.

unique curve for small enough β. For a given N and increasing β, when FCS starts to manifest itself both the exponents deviate from their long-chain values in the direction of the equilibrium value. However, in the compression direction II, the chain size soon becomes so small that a power law behavior in $S(k_{II})$ can be hardly detected. If we assume that $N = 30$ at $\beta = 10$ is still universal, the highest value we obtain for the exponent ν_I is 0.76 ± 0.04. Although it is quite plausible that ν_I would increase further with increasing β, this remains to be verified for long enough chains. In the region of small β ($\beta < 1$) the exponents differ only slightly from the equilibrium value and therefore, as discussed earlier, the theoretical predictions (13) and (14) should hold.

In Figures 11 and 12 we show, respectively, the deformation ratios $\delta G_{\alpha\alpha}$ ($\alpha = x, y, z$) and δG versus β for all chain lengths considered. In these figures, our

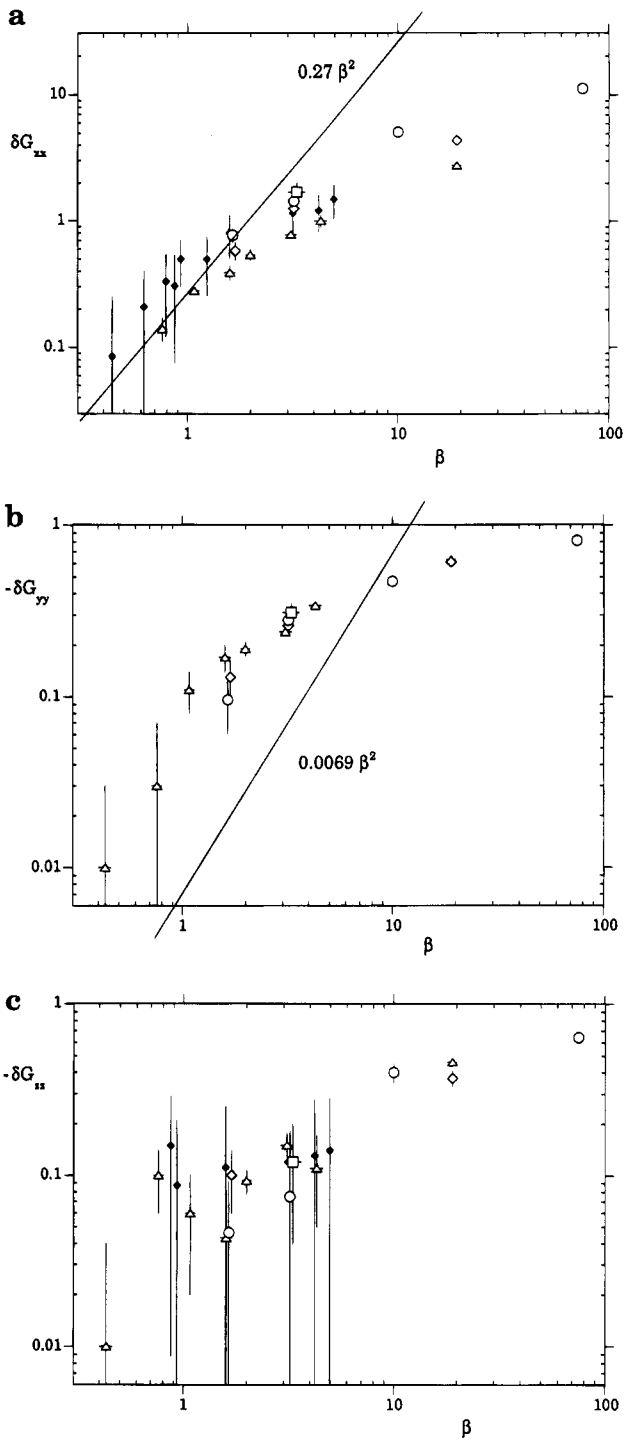

Figure 11. Deformation ratios δG_{xx} (a) and opposites of deformation ratios $-\delta G_{yy}$ (b), and $-\delta G_{zz}$ (c) versus β for all chain lengths (symbols as in Figure 10). Available SANS data for δG_{xx} and δG_{zz} are represented by filled diamonds.[2] Wang's predictions for δG_{xx} and δG_{yy} are represented by straight lines.[11]

results are compared with SANS data on polystyrene in benzene[2] whenever possible and with the theoretical predictions of Wang[11] given in Table 5. Our data for δG_{xx} (see Figure 11a) are in quantitative agreement with the SANS data[2] and it is interesting to note that both sets of data deviate from the β^2 law (14) at $\beta \gtrsim 2$. In this range of intermediate β, our data display the slight N-dependence which arises from the difference between equilibrium and nonequilibrium scaling exponents. Moreover, FCS further complicates matters in the intermediate-β region: for a given chain length N, there

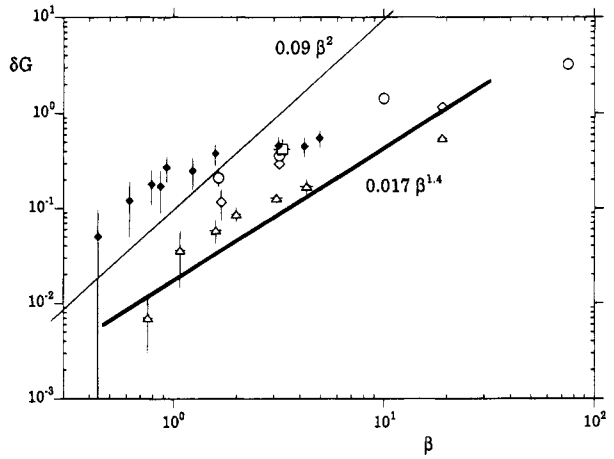

Figure 12. Deformation ratio for the trace of the gyration tensor δG versus β for all chain lengths (symbols as in Figure 10). Available SANS data are represented by filled diamonds.[2] Wang's prediction is represented by the thin line, while the thick line is the behavior $\delta G = 0.017\beta^{1.4}$ fitted to LS data.[4]

is a β value above which saturation effects disrupt the overall evolution with β: this seems to be the case, for example, for $N = 9$ at $\beta \sim 2$. This discussion demonstrates that the deformation ratios cannot be good universal indicators of the chain deformation in shear flow except in the small-β regime ($\beta < 2$) where relation (14) is found to hold. In this latter regime, the prediction of Wang[11] for the ratio δG_{xx} seems to be in a very good agreement with our data. This is not the case for the deformation ratio δG_{yy}, which at $\beta = 1$ is found to be about 1 order of magnitude larger than predicted by Wang (see Figure 11b). Two points can be made concerning this discrepancy: (i) the theoretical calculation of the deformation ratio is more difficult than for δG_{xx} because a nonpreaveraged HI model needs to be considered explicitly to obtain the correct negative sign of δG_{yy}, and (ii) there are unfortunately no experimental data to compare with. Finally, so far as δG_{zz} is concerned, Figure 11c shows a consistent picture between SANS data and simulation results, suggesting a small contraction of the chain below $\beta = 10$.

In Figure 12 we show data for the deformation ratio of the trace of the gyration tensor. We compare our results with Wang's prediction and with SANS data reported (as proposed in the experimental paper[2]) after assuming $\delta G_{yy} \sim 0$ at any β. It is clear from this figure that the overall change in the volume of the chain is much smaller than that predicted by both theory and assumed SANS data. This is due mainly to the rather large compression observed in the simulations for direction II, which partially compensates the extension in direction I. In Figure 12 we also draw the ad hoc curve $\delta G = 0.017\beta^{1.4}$ reported by Link and Springer as the best fit to their LS data for polystyrene in a Θ-solvent in the range $0.5 \leq \beta \leq 6$.[4] Such a fit cannot be exploited quantitatively because we need in that case to restrict ourselves to the β^2 regime (known through symmetry considerations to hold for small enough β). However, it is interesting to note that around $\beta = 1$ this fit suggests that the observed deformation is about 1 order of magnitude smaller than Wang's theory prediction, in agreement with our findings. The above results show that a more systematic investigation of the small-β regime needs to be carried out. In particular, it would be extremely useful to establish how the solvent quality affects the chain structure under shear in order to test the need for considering excluded volume effects in various nonequilibrium theories.

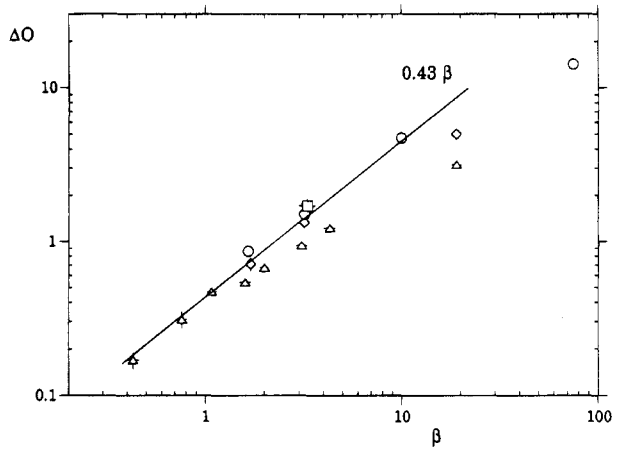

Figure 13. Amount of birefringence ΔO versus β for all chain lengths (symbols as in Figure 10). The straight line is the linear fit $\Delta O = 0.43\beta$ of data for $N = 9$ and $\beta \leq 1$.

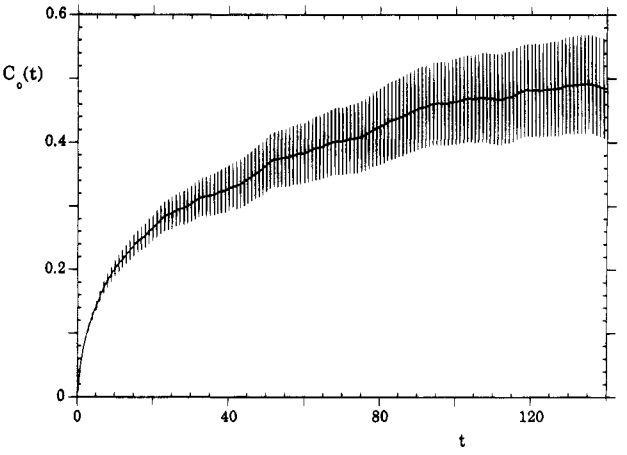

Figure 14. $N = 30$. Green–Kubo running time integral $C_0(t)$ with time expressed in single-bead (or solvent) Lennard-Jones units $\tau_{LJ} = \sigma(m/\epsilon)^{1/2}$.

Finally, for completeness, we report in Figure 13 the amount of birefringence ΔO versus β for all chain lengths investigated. The straight line is the linear fit $\Delta O = C_0\beta$ to our data for $\beta \leq 1$. Indeed, from its definition (see the beginning of section 5), ΔO starts linearly with β and the following Green–Kubo relation holds:[30]

$$C_0 = \lim_{\beta \to 0} \frac{\Delta O}{\beta} = \frac{2V}{\eta_s[\eta]_0} \int_0^\infty dt \, \langle O_{xy}(t)\sigma_{xy}(0)\rangle_{eq} \quad (15)$$

where V is the volume of the system, σ_{xy} is the microscopic stress tensor, and $\langle ... \rangle_{eq}$ indicates a statistical average for the system at equilibrium. In Figure 14 we report for $N = 30$, the running time integral $C_0(t)$ whose infinite time limit gives the value of C_0. From the figure, we estimate $C_0 = 0.48 \pm 0.08$, assuming that the expected plateau starts around $t = 100$ (note that this is the result of 11 million equilibrium steps!). Such a value agrees with the result $C_0 = 0.43$ obtained by fitting data for $N = 9$ at $\beta \leq 1$. This agreeement and the data collected in Figure 14 are certainly not in contradiction with a linear behavior $\Delta O = C_0\beta$ with an N-independent C_0 for the small-β regime. For $\beta \geq 2$, where data for different N are available, ΔO seems to exhibit a systematic N-dependence similar to that observed for the deformation ratios.

6. Conclusions

This paper is concerned with a MD study of polymers in solution subject to a steady shear flow. The originality of our approach lies in the explicit consideration of all "solvent particle" degrees of freedom in the modeling of the system. In this way, we avoid usual explict or implicit approximations which need to be made when dealing with a continuous solvent approach as in theories or in BD simulations; we think here to the handling of HI or to the validity of the fluctuation–dissipation theorem in a nonequilibrium situation. It must be emphasized that the aims of the BD and MD approaches are different. The first method consists in integrating a set of Langevin-like equations for connected monomers, i.e., the Rouse or Zimm models which are at the root of most theoretical approaches to the dynamics of nonentangled chains. Nonlinear terms (EV, nonpreaveraged HI, or finite extensibility of bonds) which prevent an analytical treatment can be included in the model since the latter is solved by techniques of stochastic dynamics. MD treats a model with explicit solvent, which is at a more fundamental level; it is intended either to simulate directly a realistic experimental situation in order to help in the interpretation of experimental data or to provide a way to test the importance of theoretical approximations required when starting from a full statistical mechanics approach. Obviously the MD approach is feasible nowadays only thanks to the recent development of computer power. It should be stressed however that BD simulation for polymers in solution with explicit HI is also not so cheap in terms of computer time. In BD the computation of the square root of the hydrodynamic matrix requires an algorithm of order N^3,[39] and as $\tau_N \sim N^{3\nu'}$ the CPU time required to follow the chain trajectory for one relaxation time grows as $N^{3+3\nu'} \sim N^{4.8}$. In the MD approach, the CPU time per step grows as $N + N_s \sim N_s$ (on a vector computer) and if we want to work at fixed R_g/L, then $N_s \sim N^{3\nu}$. Thus in MD simulations the CPU time required to follow the system trajectory for a chain relaxation time goes like $N^{3\nu+3\nu'} \sim N^{3.6}$. Of course, the prefactor is smaller in BD than in MD, but the argument above implies that BD methods are limited to quite short chains.

In the present work, we validate the MD approach in the context of polymer solutions in shear flow by showing that short chains at a given reduced shear rate deform and reorient like real (longer) chains in a Couette cell at the same reduced shear rate. This result suggests that some form of scaling must be present in the problem, just as in the usual equilibrium situation.

In our work, we propose an explicit form of this nonequilibrium scaling by investigating the self-similarities in the structure of chains of various lengths in a β-dependent rotated reference frame which is oriented along the principal axes I, II, and III of the gyration tensor $\mathbf{G}$ of the deformed polymer. The picture that emerges is as follows. At small β, the size of the chains follows a law $G_\alpha = A_\alpha(\beta)N^{2\nu}$ (α = I, II, III) where ν is the usual equilibrium Flory exponent. This scaling is compatible with the β^2 dependence of δG_{xx} and δG_{yy} often discussed in the literature. At intermediate shear rates, the scaling law must be modified to $G_\alpha = A_\alpha(\beta)N^{2\nu_\alpha(\beta)}$, where the scaling exponent ν_α depends upon the direction and is a function of β. This implies that the deformation ratios of the gyration tensor are no longer purely β-dependent quantities given the change in the scaling exponents with respect to the equilibrium value. Our anisotropic scaling interpretation is supported by a detailed analysis of the high-k regime of the chain structure factor described in section 5. The whole picture is rather well supported by the available experimental data. However, it is safe to say that given the combination of the scarcity of experiments and of the finite-chain effects described in our paper, our scaling picture at intermediate shear rates is still highly conjectural. In the present situation, we believe that further progress on these matters requires theoretical or simulation developments but, above all, systematic experiments for various chain lengths.

We note that this study is performed mainly in the intermediate-β regime ($\beta \approx 1$) where signal-to-noise problems at the low shear rates can be overcome by accumulating statistics while, at high β, we encounter saturation effects due the finite length of "short" chains and finite size effects related to the fact that as chains stretch more and more they become much larger than the simulation box. It is amusing to note that real experiments are limited to the same regime of β for very similar reasons even if real chains are somewhat longer than those that can be handled by MD! Note in this respect (i) the large error bars at small β in both simulations and experiments and (ii) the increase in chain dimensions with shear rate which leads to phase separations in real experiments[4] and boundary effects in simulations.

Comparison of our results with high-shear-rate theories cannot easily be made. The renormalization group theory predictions of Rabin and Kawasaki[14] are expected to hold at very high β ($\beta \to \infty$). Since they are based on the harmonic chain model, they probably require extremely long polymers. The situation is similar with respect to the blob model predictions of Onuki.[16] In this scheme, at large reduced shear rates ($\beta \gg 1$), chains would stretch on a large length scale and orient along the flow direction most of the time while keeping the equilibrium structure on short length scales, the transition length scale ξ_c being fixed by the absolute shear rate $\dot\gamma$. More specifically, chains would adopt an elongated structure in a coarse-grained sense where the basic units are unperturbed chain fragments (*blobs*) of n monomers whose size $\xi_c \sim n^\nu$ is fixed by the requirement that its longest relaxation time $\tau_n \sim n^{3\nu'}$ be of order $\dot\gamma^{-1}$. This leads to a number of blobs per chain N_b which depends only on β ($N_b = \beta^{1/3\nu'}$) and a number of monomers per blob which goes as $n = N\beta^{-1/3\nu'}$, where N is the chain length. In this picture the $S(\mathbf{k})$ should be isotropic and close to the equilibrium curve for $|k| \geq 1/\xi_c$ while in the flow direction it should exhibit a power law with a different slope for $|k| < 1/\xi_c$. This is indeed observed in situations for which the blob model is known to apply (for instance the case of a chain stretched by a force applied to its ends[24]). Applying the above considerations to our system, we obtain only a few blobs per chain ($N_b \sim 2$ at $\beta = 3.2$ and $N_b \sim 4$ at $\beta = 10$) which immediately indicates the mismatch between the β regime of the theory and the one of the simulation. We indeed never observe the predicted crossover in the slope of the $S(\mathbf{k})$ for $\mathbf{k}$ in the flow direction while the observed anisotropy in $S(\mathbf{k})$ extends down to the length scale of the single monomer even for $\beta \sim 1$ (see Figure 9). In conclusion, it is difficult to judge the general validity of the blob model for chains in shear flow on the basis of our data; a definite statement would require more flexible and longer chains at much higher β. It is therefore safe to conclude that

the blob model is also inadequate to interpret the available experimental data, since the latter cover the intermediate-β regime.

Further work on the simulation of chains in flows should now be directed to elongational flows (EF). The techniques described here for shear flow cannot be extended to EF since the EF can be sustained only for a few thousands of time steps, a time interval very short compared to a typical chain relaxation time. Indeed the MD cell shrinks and expands exponentially in time and sooner or later, its size in the compression direction(s) becomes smaller than the bead size! More hope could be found in mimicking in simulations the real experimental situations which have been devised to realize "model" flows.[40]

Acknowledgment. We profoundly thank I. R. McDonald for advice and a careful reading of the manuscript. Technical assistance from G. Destrée is gratefully acknowledged. The research of C. Pierleoni was partially supported by the European Community under Contract SC1*0059. We acknowledge CECAM, ENS in Lyon (France) for financial support in the final stage of this work. Computer time costs were supported by a grant from the Belgian Service de Programmation de la Politique Scientifique under Contract IT/SC/26 within the framework of the Programme National d'Impulsion en Technologie de l'Information.

References and Notes

(1) Peterlin, A. *Annu. Rev. Fluid Mech.* **1976**, 35.
(2) (a) Lindner, P.; Oberthur, R. C. *Colloid Polym. Sci.* **1988**, *266*, 886. (b) Lindner, P.; Oberthur, R. C. *Physica B* **1989**, *156 & 157*, 410.
(3) Cottrell, F. R.; Merrill, E. W.; Smith, K. A. *J. Polym. Sci., Part A-2* **1969**, *7*, 1415.
(4) Link, A.; Springer, J. *Macromolecules* **1993**, *26*, 464.
(5) Rouse, P. E. *J. Chem. Phys.* **1953**, *21*, 1272.
(6) Zimm, B. H. *J. Chem. Phys.* **1956**, *24*, 269.
(7) Carl, W.; Bruns, W. *Macromol. Theory Simul.* **1994**, *3*, 295. Bruns, W.; Carl, W. *Macromolecules* **1993**, *26*, 557.
(8) Puri, S.; Schaub, B.; Oono, Y. *Phys. Rev. A* **1986**, *34*, 3362.
(9) Wang, S. Q. *Phys. Rev. A* **1989**, *40*, 2137.
(10) Ottinger, H. C. *Phys. Rev. A* **1990**, *41*, 4413.
(11) Wang, S. Q. *J. Chem. Phys.* **1990**, *92*, 7618.
(12) Zylka, W.; Ottinger, H. C. *Macromolecules* **1991**, *24*, 484.
(13) Baldwin, P. R.; Helfand, E. *Phys. Rev. A* **1990**, *41*, 6772.
(14) Rabin, Y.; Kawasaki, K. *Phys. Rev. Lett.* **1989**, *62*, 2281.
(15) Rabin, Y.; Ottinger, H. C.; Kawasaki, K. In *Macromolecular Liquids*; Safinya, C. R., Safran, S. A., Pincus, P. A., Eds.; MRS Symp. Proc. 177; Material Research Society: Pittsburgh, 1990.
(16) Onuki, A. *J. Phys. Soc. Jpn.* **1985**, *54*, 3656.
(17) Dotson, P. J. *J. Chem. Phys.* **1983**, *79*, 5730.
(18) Liu, T. W. *J. Chem. Phys.* **1989**, *90*, 5826.
(19) Lopez Cascales, J. J.; Navarro, S.; Garcia de la Torre, J. *Macromolecules* **1992**, *25*, 3574.
(20) Knudsen, K. D.; Elgsaeter, A.; Lopez Cascales, J. J.; Garcia de la Torre, J. *Macromolecules* **1993**, *26*, 3851.
(21) Fixman, M. *J. Chem. Phys.* **1983**, *78*, 1594.
(22) Pierleoni, C.; Ryckaert, J.-P. *Phys. Rev. Lett.* **1991**, *66*, 2992; *J. Chem. Phys.* **1992**, *96*, 8539.
(23) Dünweg, B.; Kremer, K. *Phys. Rev. Lett.* **1991**, *6*, 2996; *J. Chem. Phys.* **1993**, *99*, 6983.
(24) de Gennes, P.-G. *Scaling Concepts in Polymer Physics*; Cornell University Press, Ithaca, NY, 1979. des Cloizeaux, J.; Jannink, G. *Polymers in Solution: Their Modeling and Structure*; Clarendon Press: Oxford, 1990.
(25) Doi, M.; Edwards, S. F. *The Theory of Polymer Dynamics*; Clarendon Press: Oxford, 1986.
(26) Pierleoni, C.; Ryckaert, J.-P. *Phys. Rev. Lett.* **1993**, *71*, 1724.
(27) Flory, P. J. *Statistical Mechanics of Chain Molecules*; Interscience: New York, 1969.
(28) Pierleoni, C.; Ryckaert, J.-P. *Mol. Phys.* **1992**, *75*, 731.
(29) Lee, A. W.; Edwards, S. F. *J. Phys. C* **1972**, *5*, 1921.
(30) Hansen, J. P.; McDonald, I. R. *Theory of Simple Liquids*, 2nd ed.; Academic Press: London, 1986.
(31) Pierleoni, C.; Ryckaert, J.-P. *Phys. Rev. A* **1991**, *44*, 5314.
(32) Ciccotti, G.; Ryckaert, J.-P. *Comp. Phys. Rep.* **1986**, *4*, 345.
(33) Pierleoni, C. Scaling laws in dilute polymer solution at equilibrium and in flow by molecular dynamics simulation. Ph.D. Thesis, Free University of Brussels (ULB), May 1992.
(34) Ladd, A. J. C. *Mol. Phys.* **1984**, *53*, 459.
(35) Nose, S. *Prog. Theor. Phys. Suppl.* **1991**, *103*, 1.
(36) Ciccotti, G.; Pierleoni, C.; Ryckaert, J.-P. Theoretical Foundation and Rheological Application of Non-Equilibrium Molecular Dynamics. In *Microscopic Simulation of Complex Hydrodynamic Phenomena*; Marechal, M. Holian, B. L., Eds.; Plenum Press: New York, 1991.
(37) Oono, Y. *Adv. Chem. Phys.* **1985**, *61*, 301.
(38) Yamazaki, K.; Ohta, T. *J. Phys. A* **1982**, *15*, 287.
(39) An approximate procedure which scales as $N^{2.25}$ and provides the correlated random forces needed in BD with HI has been devised. See: Fixman, M. *Macromolecules* **1986**, *19*, 1204.
(40) Odell, J. A.; Keller, A.; Rabin, Y. *J. Chem. Phys.* **1988**, *88*, 4062.

MA946148I